8

Optomechanical cooling with a nested resonator

In this chapter we show that the nested resonator design can successfully be used for optical side-band cooling. Starting from room temperature we reach an effective mode temperature of 23 ± 5 mK for a 240 kHz resonator. Careful analysis shows that the cooling limit is set by the intrinsic instability of optomechanics using a nested resonator. Although the inner and outer resonator frequencies are far apart, 240 kHz and 2.4 kHz respectively, they remain coupled as they are physically attached to each other. Therefore, the interaction of the inner resonator with the cavity field causes a large optical spring effect for the mechanical motion of the outer resonator. This can lead to a negative effective spring constant, resulting in an anti-stable mechanical system. We analyze the parameter regime where this effect occurs and discuss the consequences and possibilities for future experiments.

8.1 Introduction

Preparing a macroscopic harmonic oscillator close to its quantum mechanical ground state by means of radiation pressure cooling is one of the first steps required to perform new and interesting experiments in the field of cavity optomechanics [69, 71, 104, 41, 58]. Recently, several groups have demonstrated ground state cooling for a variety of systems [40, 39]. Furthermore, several experiments have been performed in which a mechanical oscillator was prepared in a non-classical state [90, 105, 106, 89, 46]. Another interesting prospect is the use of an optomechanical set-up to investigate the possibility of gravitational decoherence [43, 107, 8]. For this particular purpose a relatively large mass, low frequency resonator is needed together with a high quality optical cavity. These requirements make both active feedback cooling and sideband cooling have their challenges, as we will discuss below.

Active feedback cooling uses the real-time displacement of the mechanical resonator to apply a suitable feedback signal to an actuator (mechanical, optical or electrical) [108, 109, 110, 111, 112, 113]. Increasing the gain of the feedback loop results in more feedback cooling up to the point where the amplified read-out noise causes the mechanical motion to increase. This can lead to noise squashing when the mechanical displacement is monitored inside the feedback loop (in-loop measurement) [114]. To reach the quantum mechanical ground state, the initial intrinsic mechanical quality factor must be sufficiently high and the read-out sensitivity must be able to resolve the mechanical zero-point motion [30]. Recently, active feedback cooling close to the mechanical ground state has been realized in a system with read-out sensitivity significantly lower than the zero-point motion [115, 116]. Since the zero-point motion scales inversely with mass and frequency, active feedback cooling with a large mass, low frequency resonator is challenging.

We therefore opt to use optical side-band cooling instead, although this method also has its demanding requirements [117, 20]. The quality of the optical cavity must be such that the cavity linewidth κ is significantly smaller than the mechanical frequency (side-band resolved). For a free-space Fabry-Perot cavity this requires a high quality coating on both the stationary mirror and the moving end-mirror. Furthermore, the mechanical damping rate Γ_m must be small as well. This is summarized as follows: when the multi-photon cooperativity C is significantly larger than the mean phonon number of the environement, n_{th}, ground state cooling is possible. The multi-photon cooperativity C is related to experimental parameters by $C = 4g_0^2\bar{n}_{cav}/(\kappa\Gamma_m)$ with $g_0 = (\omega_{cav}/L)\sqrt{\hbar/2m\Omega_m}$ the optomechanical single-photon coupling rate, ω_{cav} the cavity resonance frequency, Ω_m the mechanical resonance frequency, L the cavity length, m the mode mass and $\bar{n}_{cav}$ the mean cavity photon number.

Recently we have shown that achieving both a small cavity linewidth and small mechanical linewidth (high Q-factor) is possible using a high quality distributed Bragg reflector (DBR) mirror together with a nested trampoline resonator design [35]. In this chapter we will demonstrate the possibilities and features of such a system. First, we demonstrate optical side-band cooling, reaching an effective temperature of 23$\pm$5 mK starting from room temperature (cooling factor of 12700). Next,

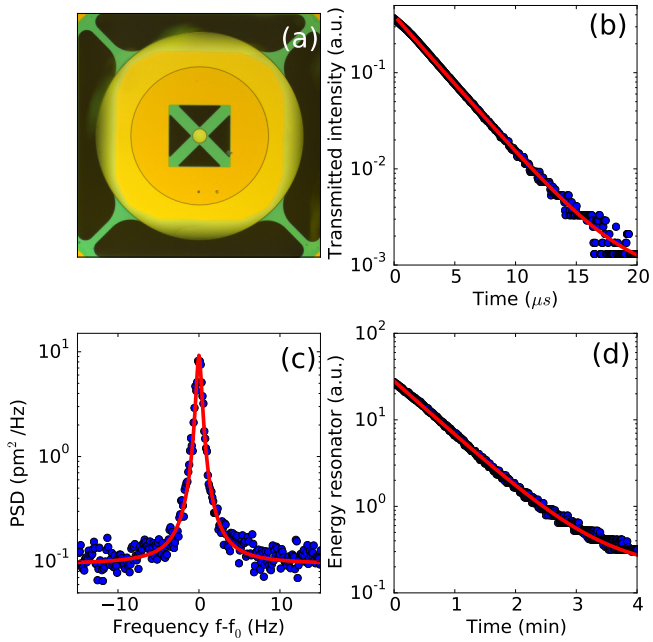

Figure 8.1: (a) Optical microscope image of the nested resonator. (b) An optical ringdown is used to obtain the cavity linewidth κ. (c) Mechanical thermal noise spectrum of the inner resonator. A mechanical quality factor of 387000 is derived from the Lorentzian fit. (d) Mechanical ringdown of the outer resonator. A quality factor of 630000 is derived from the exponential fit.

we present and discuss a model of the nested trampoline resonator to complement the results of the optical cooling experiment. Finally, we discuss the possibilities for future experiments using this design.

8.2 Optical cooling

To demonstrate optical side-band cooling with a nested resonator, we constructed a 5 cm long Fabry-Perot cavity operating around 1064 nm. The whole set-up is placed in a vibration isolated vacuum chamber and kept at a pressure below 1×10^{-5} mbar to eliminate the effect of gas damping on the mechanical properties of the resonator. Fig. 8.1(a) shows an optical microscope image of the nested resonator. An 80 micrometer diameter DBR mirror is suspended from four silicon nitride arms. This structure is surrounded by a large silicon mass suspended again from silicon nitride arms. The outer resonator acts as a mechanical low-pass filter, providing at least 60 dB of isolation for the mechanical motion of the inner resonator around its resonance frequency [35]. The inner resonator has a resonance frequency of 240 kHz and a mode mass of approximately 170×10^{-12} kg (determined via COMSOL). The outer

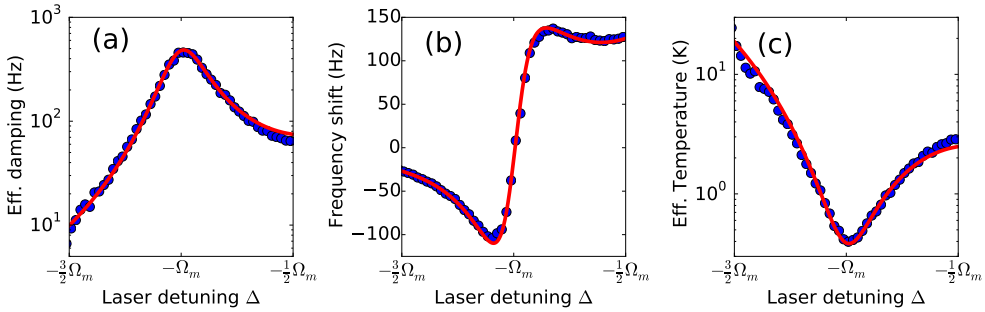

Figure 8.2: The blue datapoints are obtained via a Loretzian fit to the mechanical power spectra obtained from the PDH probe signal. The effective temperature is obtained from the integrated displacement power spectral density. The red curves are the result of a simultaneous fit to all three data-sets with only the optical linewidth and input power as free parameters.

resonator has a resonance frequency of 2.4 kHz with a mode mass of approximately 1×10^{-7} kg (determined via COMSOL).

For characterization, important optical and mechanical properties are determined via independent measurements. The optical quality of the cavity is determined via a cavity ringdown, as shown in Fig. 8.1(b). We find a cavity linewidth of 53±1 kHz. To determine the mechanical linewidth of both the inner and outer resonator, we use a laser frequency for which the DBR reflection is low (980 nm) and use a side-of-fringe lock (see Section 2.1.3) to measure the thermal motion of the mirror. Fig. 8.1(c) shows a measurement of the mechanical thermal noise spectrum of the inner resonator. From the Lorentzian fit a mechanical linewidth Γ_m of 0.62±0.03 Hz (Q-factor of 387000) is obtained. Note how clean this spectrum is by virtue of the nested system [35]. To determine the linewidth of the outer resonator a mechanical ringdown is used. The result is shown in Fig. 8.1(d). The lifetime obtained from an exponential fit gives a mechanical linewidth of 3.8±0.05 mHz (Q-factor of 630000).

The sideband-cooling experiment is carried out as follows (see chapter 5 for a more detailed description): a probe laser is kept close to the cavity resonance[1] via the Pound-Drever-Hall method [38]. The low power of the probe beam and the fact that at zero detuning no optomechanical effects occur ensures that the effects of the probe beam on the mechanical properties are minimal. A second pump laser is linked to the probe laser one free spectral range away via an optical phase locked loop. With this, the frequency difference between pump and probe laser can be set. For each specific laser detuning we measure the mechanical noise spectrum via the PDH error signal, fit a Lorentzian and extract the mechanical linewidth and frequency. The effective temperature is proportional to the total integrated area of the Lorentzian fit via the equipartition theorem since $\langle x^2 \rangle = \frac{k_B T}{m\Omega_m^2}$.

Via a relative calibration an absolute value for the effective temperature is obtained. When the pump laser is off, the resonator is assumed to be in thermal equi-

[1]To keep the system stable, the probe laser is slightly blue detuned as we will explain in the next section.

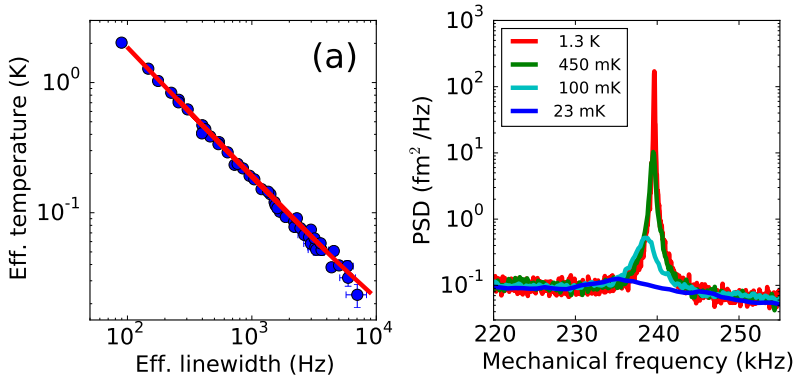

Figure 8.3: At a fixed laser detuning of $\Delta = -\Omega_m$ the intensity of the pump laser is varied. (a) The effective linewidth and effective temperature show the expected behavior. (b) Selection of mechanical noise spectra are shown to demonstrate the quality of the data.

librium with the environment at 293 K. Therefore the total integrated area of the mechanical thermal noise spectrum is set to correspond to an effective temperature of 293 K. Subsequently, when the pump laser is on, the integrated area of the measured spectrum is compared to the integrated area of the mechanical thermal noise spectrum at 293 K.

The results are shown in Fig. 8.2. The laser detuning is given in units of the inner resonator frequency Ω_m. The data, blue points in Fig. 8.2(a-c), are fitted according to the standard optomechanical theory for a single resonator (see chapters 2 and 5). The red curves show the results of a simultaneous fit to all three data-sets with only the cavity linewidth and input laser power as free parameters. An optical linewidth of κ=52.2$\pm$0.9 kHz is in agreement with the value found from the optical ringdown. The fitted value of 3.00$\pm$0.05 μW for the input laser power can be used to relate the optical power launched at the cavity to the actual power coupled to the cavity mode. This is important in the next part, where we fix the laser detuning and increase the laser power.

Fig. 8.3(a) shows the results of the side-band cooling when the cooling laser is fixed at $\Delta = -\Omega_m$ and the power is varied. The results follow nicely the expected relationship indicated by the red line. In Fig. 8.3(b) some of the mechanical noise spectra are shown. Note again that, because of the nested design, the spectra are particularly clean and free of any additional mechanical modes. For the largest pump laser power, an effective temperature of 23$\pm$5 mK is reached, starting from room temperature (cooling factor of 12700). When we try to increase the laser power even further, we observe that the system becomes highly unstable.

Although the radiation pressure only exerts a force on the small mirror, the inner and outer resonator are coupled because they are physically connected to each other. Therefore, the cavity field can still influence the motion of the low frequency outer resonator. In the next section a mechanical model of the nested resonator is discussed and we investigate if the design of a nested resonator can lead to an unstable

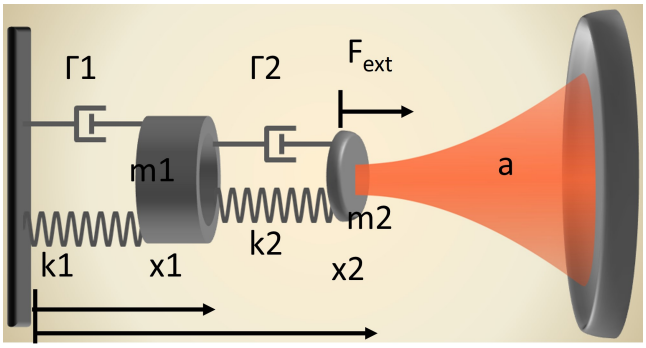

Figure 8.4: Schematic of the double resonator including relevant parameters

mechanical system for certain system parameters.

8.3 Model of a nested resonator

In Fig. 8.4 a schematic of the double resonator is shown, including relevant terms. The equations of motion for the the system are the following:

$$m_1\ddot{x}_1 + (\Gamma_1 + \Gamma_2)\dot{x}_1 - \Gamma_2\dot{x}_2 + (k_1 + k_2)x_1 - k_2x_2 = 0 \tag{8.1}$$

$$m_2\ddot{x}_2 + \Gamma_2(\dot{x}_2 - \dot{x}_1) + k_2(x_2 - x_1) - \hbar G|\alpha|^2 = F_{ext} \tag{8.2}$$

$$\dot{a} = -\frac{\kappa}{2}a + i(\Delta + Gx_2)a + \sqrt{\kappa_{ex}}s_{in} \tag{8.3}$$

in which m_i, Γ_i and k_i are the mass, damping rate and spring constant of each resonator, a denotes the cavity field amplitude, Δ the laser detuning, G the cavity frequency shift per displacement and κ_{ex} the coupling rate of the incoming field s_{in}. To find the mechanical response of the system for some applied external force F_{ext}, the cavity field equation can be linearized using $a = \bar{a} + \delta a$ (similar to the approach in chapter 2). By taking the Fourier transform, collecting terms and rewriting using $k_i = \Omega_i^2 m$ the following three equations are obtained:

$$x_1[\omega](m_1(\Omega_1^2 - \omega^2) + m_2\Omega_2^2 - i\omega(m_1\Gamma_1 + m_2\Gamma_2) - x_2[\omega](\Omega_2^2 m_2 - i\omega m_2\Gamma_2) = 0 \tag{8.4}$$

$$x_2[\omega](m_2(\Omega_1^2 - \omega^2) - i\omega m_2\Gamma_2) - x_1[\omega](m_2\Omega_2^2 - i\omega m_2\Gamma_2) - \hbar G(\bar{a}^*\delta a[\omega] + \bar{a}\delta a[\omega]^*) = F_{ext}[\omega] \tag{8.5}$$

$$-i\omega\delta a[\omega] = (i\Delta - \kappa/2)\delta a[\omega] + iG\bar{a}x_2[\omega] \tag{8.6}$$

Now Eqs. (8.4) and (8.6) can be used to rewrite Eq. (8.5) in the following form: $x_2[\omega]\chi_2^{-1} = F_{ext}[\omega]$ with χ_2 the mechanical susceptibility of mass 2, the inner resonator. The result is the following:

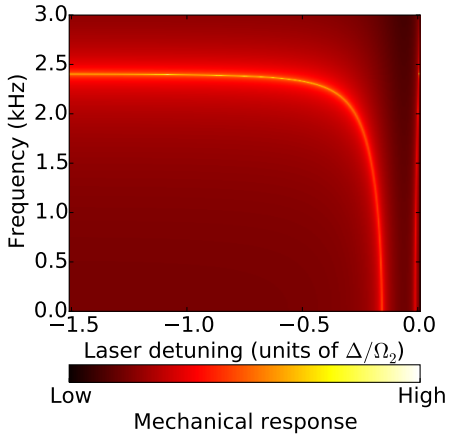

Figure 8.5: Mechanical response of the outer resonator as function of laser detuning.

$$x_2[\omega]\Big(m_2((\Omega_2^2-\omega^2)-i\omega\Gamma_2)+ 2m_2\Omega_2 g^2\big(\frac{1}{\Delta+\omega+i\kappa/2}+\frac{1}{\Delta-\omega-i\kappa/2}\big) - \frac{m_2(\Omega_2^2-i\omega\Gamma_2)}{m_1(\Omega_1^2-\omega^2)+m_2\Omega_2^2-i\omega(m_1\Gamma_1+m_2\Gamma_2)}\Big) = F_{ext}[\omega] \quad (8.7)$$

The multi-photon coupling rate $g^2 = \hbar G^2|a|^2/(2m_2\Omega_2)$ is introduced to simplify the equation. The inverse susceptibility χ_2^{-1} contains three terms (note the linear nature of the mechanics). The first term is the response of a damped harmonic oscillator. The second term is the optomechanical interaction. This term is identical to the case of a single mechanical resonator (see chapter 2). The real part results in the familiar optical spring effect and the imaginary part gives the optical damping. The final term is the coupling with the outer resonator. From χ_2 the amplitude response of the inner resonator is extracted by $|\chi_2|$ and the phase response by $\arg(\chi_2)$.

We are however interested in the mechanical response of the outer resonator. Combining the result of Eq. (8.7) with Eq. (8.4) we find the following:

$$\chi_1 = \chi_2 \frac{m_2(\Omega_2^2-i\omega\Gamma_2)}{m_1(\Omega_1^2-\omega^2)+m_2\Omega_2^2-i\omega(m_1\Gamma_1+m_2\Gamma_2)} \quad (8.8)$$

As before the amplitude and phase response of the outer resonator are found via the magnitude and argument of χ_1.

Now the response of the nested resonator can be investigated. Fig. 8.5 shows the mechanical response of the outer resonator as a function of laser detuning. The same values are used as for the measurements of Fig. 8.2. For a laser detuning of $\Delta = -1.5\Omega_2$, the resonance frequency of the outer resonator is still unaffected by the

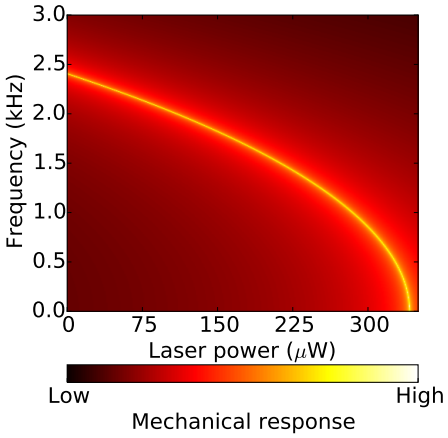

Figure 8.6: Mechanical response of the outer resonator as function of laser power for a fixed detuning of $\Delta = -\Omega_2$.

optical field. In the region between $\Delta = -0.5\Omega_2$ and $\Delta = 0$, the mechanical resonance frequency slowly decreases to zero, as indicated by the yellow line in Fig. 8.5. For the outer resonator, the optomechanical system is highly non side-band resolved, therefore a large optical spring effect is not surprising. The outer resonator experiences this optical spring effect via the coupling to the mirror of the inner resonator. Therefore the nested resonator can be considered a single mechanical oscillator at low frequencies.

In the region between $\Delta = -0.2\Omega_2$ and $\Delta = 0$, the optical spring effect has reduced the mechanical frequency to zero. Furthermore, the optical spring effect is so large that the system has a negative spring constant. This leads to an anti-stable system, as has been demonstrated by Corbitt et al. [75]. We have verified this behavior experimentally. Placing the pump laser between $\Delta = -0.2\Omega_2$ and $\Delta = 0$ results in an unstable mechanical system.

A similar instability is observed when the laser power is increased. This was the main limitation in the experiment of Fig. 8.3. We can therefore also investigate the mechanical response when the laser detuning is fixed at $\Delta = -\Omega_2$ while varying the laser power. The results are shown in Fig. 8.6. The same values are used as for the measurements of Fig. 8.3. For a single resonator the optical spring effect increases with power. It is therefore not surprising that for high laser powers at $\Delta = -\Omega_2$ a significant optical spring effect occurs for the outer resonator.

It is not uncommon for undesired effects, such as heating of the mechanical system due to optical absorption or excess laser noise, to appear at high laser powers [71, 118]. These effects typically limit the effective temperature reached with side-band cooling. In the case of a nested resonator, the mechanics of the design itself places an upper limit on the amount of laser power that can be used. This can potentially be an issue for future experiments. However, achieving a cooling factor of 13000 before the design of the nested resonator became a limiting factor suggests

that the issue it not likely to be a deal-breaker for reaching the quantum mechanical ground state. Should a solution be needed, the resonance frequency of the outer resonator can be increased. A drawback of this solution is the reduction in isolation of the inner resonator from the environment. An alternative route would be to implement additional control of the motion of the outer resonator. This can be done electrically via capacitive coupling or via the dielectric force [119] or even optically using additional laser beams [75].

Another motivation for additional control over the motion of the outer resonator is the high mechanical quality factor. The low frequency of the outer resonator, needed to provide sufficient isolation, can be easily excited by the boiling of cryogenic liquids or the presence of cryocoolers. Together with the high mechanical quality factor this can lead to a significant displacement of the outer resonator. Since the amount of isolation does not depend on the mechanical quality factor [35], additional damping can be applied via an active feedback method, to reduce the quality factor but still keep the mechanical isolation. The next chapter investigates active feedback cooling as a method to control the motion of the outer resonator.

8.4 Conclusions

With the recent introduction of the nested trampoline design, both good optical and mechanical properties are combined in a relatively low frequency high mass optomechanical device. We have demonstrated in this chapter that such a device can successfully be used for optical cooling experiments, reaching an effective temperature of 23 ± 5 mK starting from room temperature. The cooling performance turns out to be limited by a large optical spring effect acting on the outer resonator. The resonance frequency is lowered close to zero, leading to a system which is very vulnerable to low frequency noise.

An attractive solution would be to add additional control over the motion of the outer resonator. Not only can this be used to counteract the optical spring effect, but the outer resonator can also be damped to reduce the mechanical quality factor. This reduces the movement of the outer resonator due to external forces when the set-up is placed in a noisy, cryogenic environment, which is required for reaching the quantum mechanical ground state.